Metallic wool for enhanced thermal conductivity of phase change materials

Audrey Favache[a,*], Pierre Bollen[a], Xavier Bollen[a], Gilles Baudoin[c], Thomas Pardoen[a]

[a] Institute of Mechanics, Materials and Civil Engineering, Université catholique de Louvain, Place Sainte Barbe 2 – L5.02.02, 1348 Louvain-la-neuve, Belgium

[c] Louvain research institute for Landscape, Architecture, Built environment, Université catholique de Louvain, Place du Levant 1 – L5.05.04, 1348 Louvain-la-neuve, Belgium

* Corresponding author (Audrey.favache@uclouvain.be)

Abstract

The heat transfer potential of Phase Change Materials (PCMs) is augmented by insertion of a metallic wool with high thermal conductivity. Apparent thermal heat conductivity has been determined experimentally in the solid and in the liquid phase for different wool contents. Heat transfer is enhanced by the addition of wool in solid phase, but is mitigated in liquid phase by the restriction of natural convection. The difference in heat transfer efficiency in the liquid and solid phase induces an asymmetric behavior between the melting and solidification configurations. The behavior of metallic wool-PCM composites is very similar to metallic foam-PCM hybrids studied in literature. As shown on the basis of rationale material selection, the addition of a metallic wool constitutes in the practice a cost and process effective way to control the heat transfer potential.

Keywords

Phase change material, metal wool, natural convection, heat transfer

1. Introduction

The global warming problem has generated a growing interest towards new solutions for better energy management, especially energy coming from non-controlled sources, e.g. solar energy, wind energy etc. One disadvantage of many of these solutions is the temporal mismatch between energy production and needs. Hence, energy production must be dissociated from energy consumption by the means of energy storage systems. The problem of temporal mismatch between production and needs is not limited to electrical energy, but also impacts heat or cold production and needs, which motivates the development of thermal storage systems.

Phase Change Materials (PCM) based technologies are receiving a growing attention. In PCMs, the phase-transition latent energy is the working principle for storing large amounts of thermal energy in a small window of temperature variations compared to specific energy. There are several classes of PCMs differing among others in the type of phase change, in the range of temperature of the phase transition and in the constituent (type of) material. Liquid-solid PCMs are very much used for their high energy storage capacity together with a restricted volume change. PCMs are often classified as eutectic PCMs, organic PCMs and inorganic PCMs [1]. The optimal choice of PCM depends on the application, but most of them suffer from a low thermal conductivity, which significantly restricts the effectively used material volume for energy storage over the appropriate time periods or the allowable input/output power. Hence, a large number of researches on PCMs has been focused on heat transfer enhancement [2]. The methods are

based either on heat transfer enhancement by system design (e.g. fins, heat pipes) or on compounding the poorly conductive PCM with a highly conductive material such as metallic foams [3,4], carbonated foams [5,6] or dispersion of conductive particles [7–10]. Blending with particles does not give as good results as continuous matrices due to sedimentation problems and a lack of percolation [11]. Foams are expensive and infiltration by the PCM is often difficult, requiring sometimes vacuum infiltration [4,12,13].

Extensive studies have been performed about the heat transfer in composite PCMs with conductive fillers, mostly foams [12,14–18]. Especially, it has been shown that convection phenomena improve the effective heat transfer in pure liquid PCM, while the presence of a foam limits the amplitude of this effect [3,19]. More precisely, convection is controlled by the foam porosity [16–18], while the pore size has minor [17,20] to no effect [12,16]. Most of these studies focus on the melting process with the solidification addressed only in a few investigations, as for instance in [3,19,21].

In the present study, the selected working principle for enhancing the heat transfer potential is the hybridization with a metallic wool or felt. This approach potentially offers the advantage of involving a percolating heat conduction path, but at a lower cost and easier manufacturing conditions compared to graphite or metallic foams widely considered in the literature. Indeed, the production of metal foams requires the melting of the metal and the use of blowing agents or sacrificial materials (lost foam casting) [22] whereas the processing of metal wools mainly follows mechanical principles [23]. A metal wool can also be fitted in complex shapes without the need of machining. A more detailed comparison of the use of metallic fibers with other thermal conductivity enhancement techniques can be found in [24].

Despite the advantages of the use of metallic wool, a small number of researches have addressed this class of this hybrid material [24–28]. Even if the competing mechanisms between conduction and convection similar to the case of the addition of foams are expected to take place when adding a metallic wool, only very few studies have carefully addressed this option. Wang et al. investigated the addition of sintered metal felts for enhancing the performances of heat sinks [25]. Different compositions were tested in melting configuration, but no quantitative characteristic of the heat transfer was provided. In [28], the authors used a composite made of micro-encapsulated PCM together with aluminum or steel wool to produce panels for building applications. An increase of about 1 to 6% of the thermal conductivity of the panel was determined for wool ratios between 2 and 3%. However, this study evaluated the apparent conductivity of the entire panel, and not of the compound alone. Moreover, the micro-encapsulation of the PCM will affect the appearance of natural convection mechanisms. Gasia et al. looked at the addition of a metallic wool compared to fins and concluded that wool is less effective than fins, but it is cheaper and easier in terms of the charging process [27]. A similar work has been conducted by Youssef at al. in the framework of a solar distillation system [29]. The more recent study of Prieto et al. focused on the use of metal wool hybridized PCMs for industrial solar heat applications [24]. The interest of using wool was confirmed with an increase of 300% of the thermal conductivity in comparison to pure PCM.

The present study is in line with a recent work on metallic wool [24] with the aim to determine the impact on the use of metallic wool as a heat transfer enhancement method. For this purpose, the apparent heat conductivities have been determined experimentally as a function of the wool content both in solid and liquid phase, and compared to experimental values for composites from literature and to composite mixing rules. This

is complementary to the analysis of Prieto et al. [24], in which the apparent thermal heat conductivities in solid phase is estimated as a rule of mixture and only a coarse order of magnitude is given for the liquid phase, and this for only one wool content. Moreover, contrary to the previous work on metallic wool composites, the one novelty of this study is that the asymmetry between the charge and discharge processes due to the convection effects is discussed with visual observations of the fusion front. Since the present study takes place in the context of building applications, the experiments have been conducted on paraffin-based PCM slightly above room temperature, whereas the study of Prieto et al. uses inorganic salt at around 200°C. In building applications, the objective of adding PCM is to store the most possible of the thermal energy entering during daytime, while being able to release all of it during night. With regard to this, the benefit owing to the addition of wool in both charging and discharging configurations is analyzed in the framework of a rationale material selection approach [30]. In order to achieve our objectives, an experimental set-up allowing both quantitative measurements of the apparent thermal conductivity and phase change visualization has been designed. This setup is presented in Section 2, together with the analytical data reduction scheme to assess the apparent thermal conductivity. Section 3 describes the results which are discussed in Section 4, before final conclusion.

2. Materials and methods

2.1. Experimental set-up

The hybridized PCM was tested via a home-made setup illustrated in Figure 1. The material is placed inside a half-cylinder-shaped aluminum container of 10 cm diameter and 3 mm thickness (at thinnest). To conform to a building cooling application, a

controlled heat flow is imposed similarly to [24]. This has been achieved using 12 Peltier elements from TEC Microsystems of 3.3 W maximum cooling power each, fixed in two rows inside a 3D printed nylon holder, allowing to work in both heating and cooling modes. The heat flow is determined by the current applied through the elements. A membrane heater of 150W was positioned at the rear of a copper block which plays the role of a buffer and of a heat spreader. In heating mode, the heater is activated by a Siemens controller to keep the two faces of the Peltier elements at the same temperature. This ensures that the heat flux through the Peltier elements is kept constant during the whole experiment and that there is no heat loss towards the copper block. Homogeneous heat flow and a good contact with the Peltier elements is ensured by graphite thermal interface sheets inserted between the Peltier elements and the aluminum container on the one side, and the copper block on the other side. The melting front can be optically monitored owing to a double-glazing front window. The bottom and the top of the container are filled with a polyurethane foam so that heat can only enter or exit the container through the lateral walls and unwanted heat flows are reduced to a minimum. The entire setup is entirely surrounded by polyurethane plates for thermal insulation. When not taking pictures, the window is sealed with polyurethane foam as well. The double-glazing window and its additional insulation ensure an axisymmetric configuration so that the set-up behaves as a full cylinder. Heat loss coefficients through the front face have been evaluated by natural cooling down of the samples while using the regulated thermal resistance for the copper block temperature to follow the temperature of the aluminum, ensuring an active isolation of the periphery. All experiments have been conducted such that the thermal losses are less than 5% of the heat flow entering the PCM.

The temperature of the faces of the Peltier elements is monitored by 6 thermocouples located on each side of the nylon mold containing these elements. The temperature profile inside the hybridized PCM is determined owing to 13 thermocouples inside the test material, at half height.

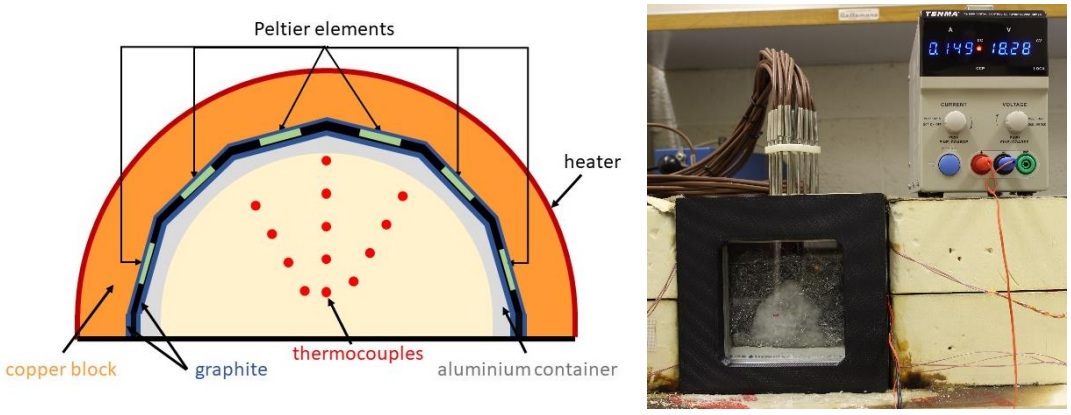

Figure 1: (left) Schematic top view representation and (right) picture of the experimental set-up.

The heat flow has been calibrated under heating mode using demineralized water filled inside the setup. This allows relating the current through the Peltier elements to the heat flow transferred from the copper block to the aluminum container.

Solidification experiments have been performed by withdrawing the insulation around the container to ensure radial outgoing heat flow. Hence, cooling comes only from natural convection between the copper block and the ambient air. The room was climatized with a control thermocouple confirming a constant room temperature of 18.3 ± 0.5°C.

2.2. Materials

The test material is a compound made of organic PCM infiltrated into an aluminum wool at several mixing ratios. The PCM is the paraffin RT28HC from Rubitherm. It has a melting temperature around 28°C. The datasheet provided by the supplier indicates a

thermal conductivity of 0.2 W/(m·K). Differential scanning calorimetry (DSC) performed on 26.2 mg of PCM gives a heat capacity ranging from 1.2 to 1.8 kJ/(kg·K) and a phase change enthalpy of 253 kJ/kg. The metallic wool is a coarse graded aluminum wool from Piwel with fiber diameter approximately equal to 100 µm.

The hybridized material was produced by putting the aluminum wool into the experimental set-up in the most homogeneous way. Then, the liquid PCM was filled into the set-up up to a fixed level of 8 cm. The amount of PCM was measured both by weighting the PCM container before and after filling, and from the weight of the full composite made of aluminum and infiltrated PCM, which is withdrawn from the set-up in solid state after the experiments. A complete solidification-melting-solidification cycle is performed for running in before testing in order to ensure a good contact between the PCM and the thermocouples. No specific procedures have been necessary to impregnate the wool, even for 18% mass wool content, contrary to what has been reported in [31], indicating the simplicity of the process associated with the low viscosity of the liquid paraffin. The different tested compositions and the list of thermal characterization experiments is given in Table 1.

Table 1 : Experimental conditions of the experiments on the paraffin/wool composites. Measurements marked with an asterix have been repeated at least 2 times to check for repeatability.

Sample	**RT28HC**	**RT28HC-9.5Al**	**RT28HC-9.8Al**	**RT28HC-18Al**
Composition				
Mass PCM [g]	*260*	*257*	*248*	*236*
Mass Al wool [g]	-	27	27	52
% mass Al	0.0	9.5	9.8	18.2
Actual mean density (solid state) [kg/m³]	783 ± 5	951± 10	973± 8	870±12
Actual mean density (liquid state) [kg/m³]	778±10	940 ± 5	947± 6	867±10
Equivalent porosity [%]	100	96.7	96.5	94.2
Applied current during the thermal experiments without phase change				
Solid state	0.075 A*	0.075 A	0.15 A	0.15 A
Liquid state	0.15 A	0.15 A	0.15 A	0.15 A
Applied current during the thermal experiments with phase change				
Melting configuration	0.15 A 0.25 A	0.15 A		0.15 A 0.25 A

2.3. Data reduction scheme for the determination of thermal conductivity

The dynamics of the set-up without phase change is analyzed in order to identify the apparent thermal conductivity of the hybridized PCM. The symbols and notations are given in Table 2.

The heat equation in cylindrical coordinates is given by $\rho c_p \frac{\partial T}{\partial t} = k \frac{1}{r} \frac{\partial}{\partial r}\left(r \frac{\partial T}{\partial r}\right)$, along the radial coordinate *r*. Assuming perfect insulation at the front face of the half-cylinder, the boundary conditions are governed by the incoming heat flows $\left.\frac{\partial T}{\partial r}\right|_{r=0} = 0$ and

$k\left.\frac{\partial T}{\partial r}\right|_{r=R} = \frac{Q^{in}}{\pi R h}$s, where R is the radius of the aluminum container and h the height of the specimen. For constant Q^{in}, the solution of the heat equation is given by the following relationship:

$$\begin{aligned} T(r,t) - T_0(r) \\ = \frac{Q^{in}}{mc_p}t + \left(\left(\frac{r}{R}\right)^2 - \frac{1}{2}\right)\frac{Q^{in}}{2k\pi h} \\ + \frac{Q^{in}}{\pi R h}\sum_{i=1}^{\infty}\alpha_i e^{-\frac{D\lambda_i^2}{R^2}t} J_0\left(\frac{r}{R}\lambda_i\right), \end{aligned} \tag{1}$$

where $D=k/(\rho c_p)$ is the thermal diffusivity, $J_0(x)$ is the Bessel function of the first kind, α_i are determined from the initial conditions at t=0 and λ_i are the roots of the Bessel function $J_1(x)$.

Inserting the global energy balance $\frac{dT_{mean}(t)}{dt} = \frac{Q^{in}}{mc_p}$ into equation (1) leads to the following equations for the temperature profile inside the test material, assuming homogeneous initial temperature in the specimen:

$$\frac{T(r,t)-T_{mean}(t)}{Q^{in}} = \left(\left(\frac{r}{R}\right)^2 - \frac{1}{2}\right)\frac{1}{2k\pi h} + \frac{1}{\pi R h}\sum_{i=1}^{\infty}\alpha_i e^{-\frac{D\lambda_i^2}{R^2}t} J_0\left(\frac{r}{R}\lambda_i\right), \tag{2}$$

or

$$\begin{aligned} \left(T(r,t) - T_{mean}(t)\right)\left(\frac{dT_{mean}(t)}{dt}\right)^{-1} \\ = \left(\left(\frac{r}{R}\right)^2 - \frac{1}{2}\right)\frac{R^2}{2D} + \frac{mc_p}{\pi R h}\sum_{i=1}^{\infty}\alpha_i e^{-\frac{D\lambda_i^2}{R^2}t} J_0\left(\frac{r}{R}\lambda_i\right). \end{aligned} \tag{3}$$

It is important to mention that the Peltier elements maintain a constant heat flow $Q^{Peltier}$ which differs from Q^{in} by the power stored in the aluminum container when neglecting thermal losses. Assuming a homogeneous temperature inside the aluminum container, the heat flow into the test specimen is simply

$$Q^{in} = Q^{Peltier} - m_{container} c_{p,container} \frac{dT_{container}}{dt}. \quad (4)$$

In the same way as inside the PCM, the temperature of the aluminum container evolves linearly with time after a transition regime, so that Q^{in} becomes constant.

The above development guides the design of experiment and the data reduction scheme for the determination of the apparent heat capacity and thermal conductivity of the test material. The proposed data reduction scheme without phase change is hence as follows:

- D is extracted from the slope of $\left(T(r,t) - T_{mean}(t)\right)\left(\frac{dT_{mean}(t)}{dt}\right)^{-1}$ versus $\left(\left(\frac{r}{R}\right)^2 - \frac{1}{2}\right)$. After some stabilization time, the second term of equation (3) becomes indeed negligible, so that the relationship becomes constant with the slope related to the inverse of D.
- k is calculated from the experimental value of D since $k=\rho D c_p$. Note that k could also be extracted from the slope of $\frac{T(r,t)-T_{mean}(t)}{Q^{in}}$ versus $\left(\left(\frac{r}{R}\right)^2 - \frac{1}{2}\right)$. After some stabilization time, the second term of equation (2) becomes indeed negligible, so that the relationship becomes constant with the slope related to the inverse of k. The advantage of the first calculation is that it is independent of the knowledge of the magnitude of the input heat flow and hence not sensitive to errors in the calculation of Q^{in}, contrary to the second one.

The thermal conductivities and diffusivities which will be obtained using the above reduction scheme are apparent conductivities and diffusivities. Indeed, the analytical model assumes pure conduction whereas natural convection may take place in the experiment. Improvement of the heat transfer due to natural convection will hence lead to apparently higher conductivity and diffusivity.

1 *Table 2 : Symbols and notations*

Symbols		Subscripts and exponents	
c_p	Heat capacity	*container*	aluminum container
D	Thermal diffusivity	*ext*	At the external boundary of the PCM
$\Delta_f H_{PCM}$	Phase change energy per unit mass of pure PCM	*mean*	Mean over the sample
h	Sample height	*PCM*	Pure (non hybrided) PCM
k	Thermal conductivity	*0*	at t=0
m	Sample mass		
m_{PCM}	Mass of PCM contained in the sample		
Q^{in}	Heat flow from the aluminum container into the sample		
$Q^{Peltier}$	Heat flow entering the aluminum container imposed by the Peltier elements		
r	Radial coordinate		
R	Radius of the container		
ρ	Sample density		
t	time		
T	temperature		

2

2.4. Finite element model

Although the previous analytical model leads to a data reduction scheme for extracting the thermophysical properties of the sample, there is no analytical solution when phase change is taking place. Therefore, a 2D finite element model has been built and solved using the transient thermal analysis solver of the PDE toolbox of MatLab in order to simulate the temperature field in the PCM. The aim of the FE model is to give a phenomenological insight when phase change occurs. The boundary condition is the total ingoing heat flow into the sample by external surface unit area. By symmetry of the container, only one half (hence a quarter of cylinder) has been modelled. The mesh contains 3200 quadratic elements and is illustrated at Figure 2. Phase change has been modelled using a temperature dependent heat capacity depending on the temperature. In order to determine solely the effect of the difference in the heat transfer efficiency, a symmetric enthalpy curve centered on the fusion temperature has been used and the values for c_p outside the phase change region and ρ are kept constant. Phase change temperature range and enthalpy have been taken equal to the values from the DSC results of the real PCM (see Figure 2). A convergence analysis has been performed to ensure sufficient spatial and temporal mesh refinement.

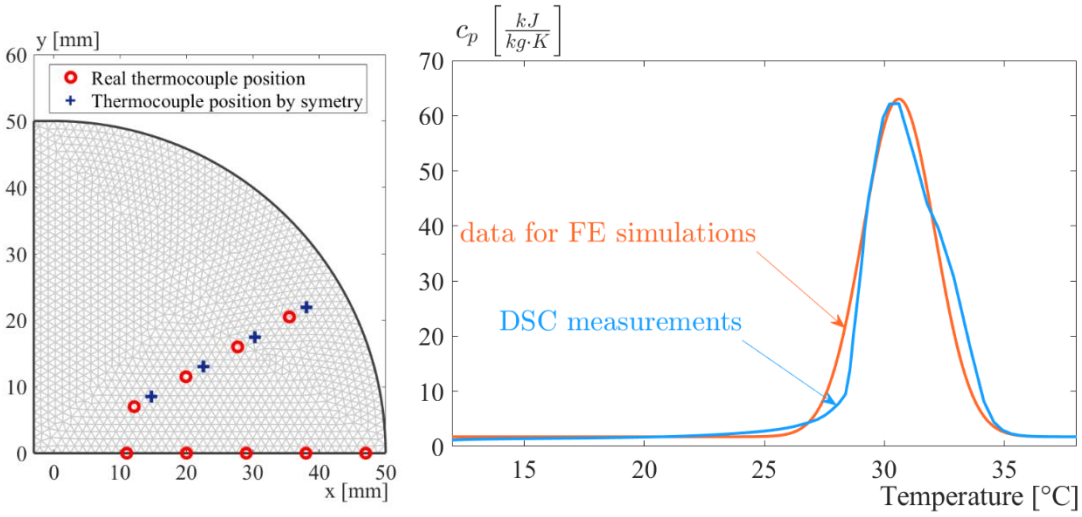

Figure 2: FE model of the PCM: (left) Mesh. The positions of the thermocouples are indicated by the markers. (right) Temperature dependent heat capacity.

3. Results

The heat flow entering the PCM is calculated using eq. (4) and displayed in Figure 3. For readability of the figure, only experiments at 0.15 A have been displayed.

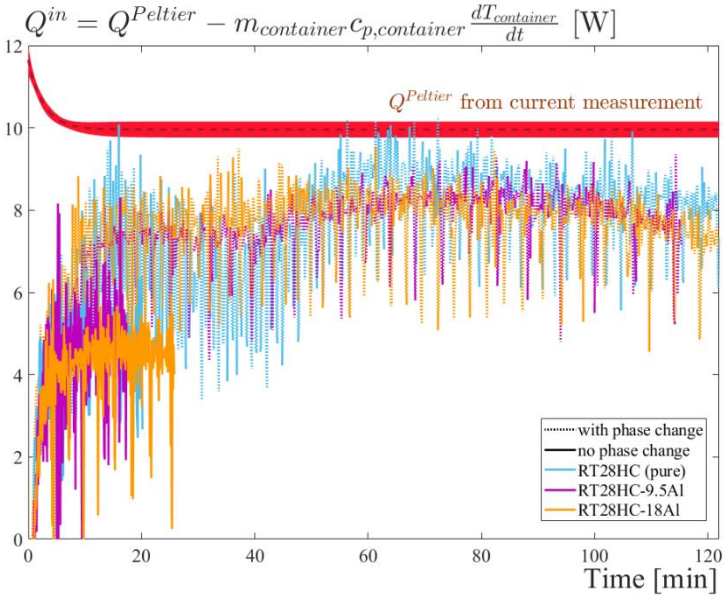

Figure 3: Ingoing heat flow in the PCM as calculated by eq. (4) in the experiments without and with phase change (set point for current through the Peltier elements: 0.15 A).

3.1. Thermal response without phase change

The experiments without phase change (see Table 1) have been performed in order to assess the thermal characteristics of the hybridized PCMs in solid and in liquid phase.

The procedure described in Section 2.3 has been used to estimate the thermal diffusivity and thermal conductivity. Figures 4 and 5 illustrate the procedure for the PCM in liquid phase involving 9.5% of Al wool. Figure 4 shows the time evolution of the temperature determined by the different thermocouples inside the PCM and at the exterior of the container. As expected from equation (1), after a transitory regime of approximately 10 min, the temperatures at each of the measurement points evolve in parallel. Figure 5(a) represents the temperature profile as extracted from equation (3) while Figure 5(b) shows the value of D extracted from the slope of the linear interpolation as a function of time.

Indeed, after the transient regime, the profiles of Figure 5(a) superimpose and a constant value for D is found.

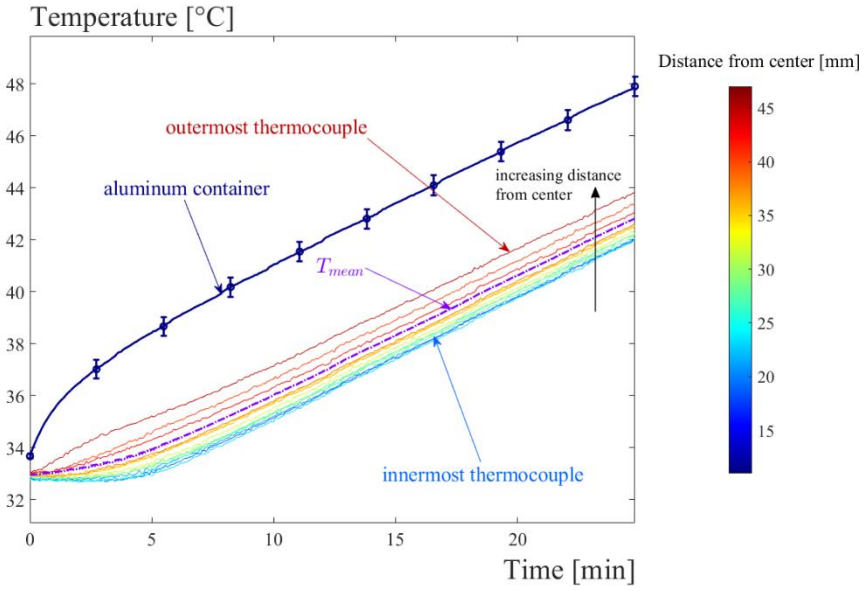

Figure 4: Temperature evolution during the heating of RT28HC-9.5Al.

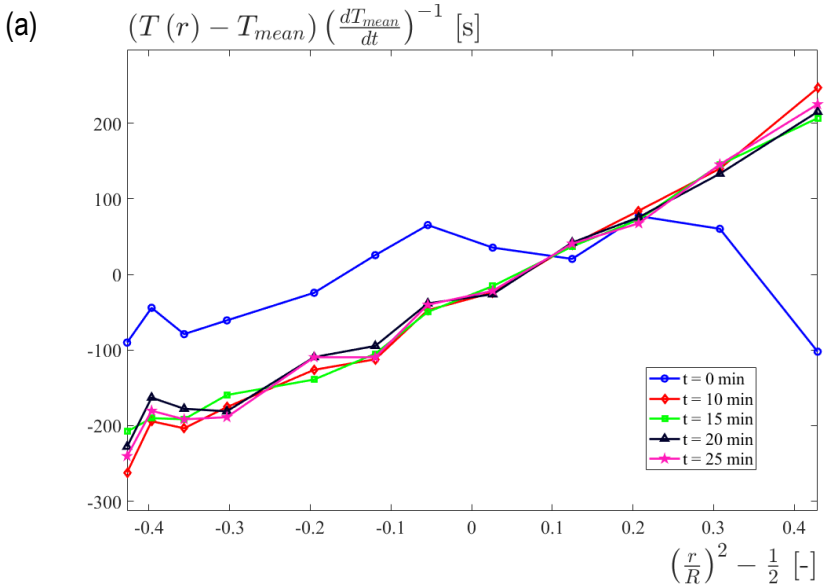

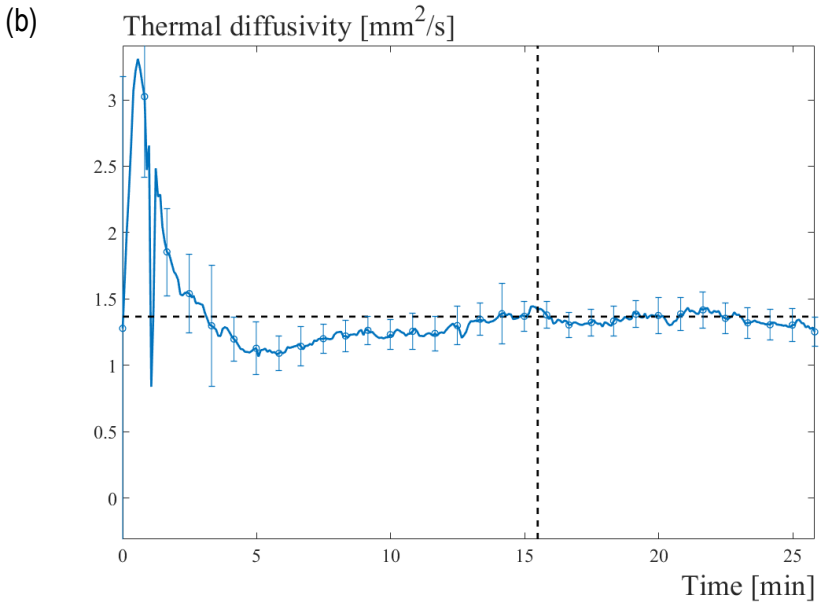

Figure 5: Illustration of the procedure to estimate the thermal diffusivity. (a) Temperature profile at different times. Quantities are normalized as suggested from the form of equation (3); (b) Thermal diffusivity estimated from the slope of Figure 5(a).

Thermal conductivity may then be calculated from the experimental value of D through $k=\rho c_p D$. The values of ρ have been measured from the volume occupied in the set-up (Table 1). The c_p values as a function of temperature have been calculated by a simple law of mixture using the experimental DSC values for the pure RT28HC and 0.89 kJ/(kg·K) for aluminum. The c_p values from DSC are then averaged over the temperature range in which calculation of k is performed. The results are presented in Table 3.

Table 3 : Thermophysical properties of the different hybridized PCM

% mass Al	c_p [kJ/(kg K)]	D [mm²/s]	$k = D\,\rho c_p$ [W/(m K)]
Solid state			
0.0	1.3 ± 0.1 1.49 ± 0.03 1.41 ± 0.09	0.46 ± 0.07 0.39 ± 0.08 0.39 ± 0.04	0.51 ± 0.08 0.49 ± 0.07 0.52 ± 0.06
9.5	1.1 ± 0.4	1.19 ± 0.14	1.65 ± 0.17
9.8	1.36 ± 0.07	1.25 ± 0.18	1.76 ± 0.26
18.0	1.3 ± 0.1 1.3 ± 0.1	1.49 ± 0.16 1.53 ± 0.16	1.81 ± 0.17 1.95 ± 0.19
Liquid state			
0.0	1.81 ± 0.06 1.80 ± 0.04	10 ± 7 9 ± 5	14 ± 9 13 ± 7
9.5	1.76 ± 0.05	2.3 ± 0.6	4.0 ± 1.0
9.8	1.70 ± 0.02	1.8 ± 0.6	3.7 ± 1.4
18.0	1.70 ± 0.05 1.63 ± 0.03	1.35 ± 0.12 1.17 ± 0.13	1.81 ± 0.18 1.72 ± 0.17

3.2. Thermal response with phase change

The pictures taken during the melting experiments are displayed at Figure 6. The temperature measurements are shown in Figure 7, while Figure 8 displays the evolution of the melting process. In order to take into account that the hybridized PCM samples contain less RT28HC, time has been normalized by the time for full PCM melting as if the temperature were homogeneous, namely $t_{melt} = \frac{m_{PCM}\Delta_f H_{PCM}}{Q^{in}}$, where $\Delta_f H_{PCM}$ is the phase change latent energy of pure PCM. Moreover, the initial time has been shifted in order to take into account that the initial temperature slightly differed between the experiment such that t=0 corresponds to the same energy content:

$$t = t_{mes} - \frac{mc_p(T_{init} - T_{ref})}{Q^{in}}$$

where T_{ref} is the reference temperature here taken as the initial temperature of the experiment with the lowest initial temperature and t_{mes} is the time from the beginning of the experiment. The solidification experiments have been performed by letting the set-up cool down freely. Figure 9 shows the temperature measurements. Time has been normalized by the amount of phase-change energy present in the sample, namely $m_{PCM}\Delta_f H_{PCM}$.

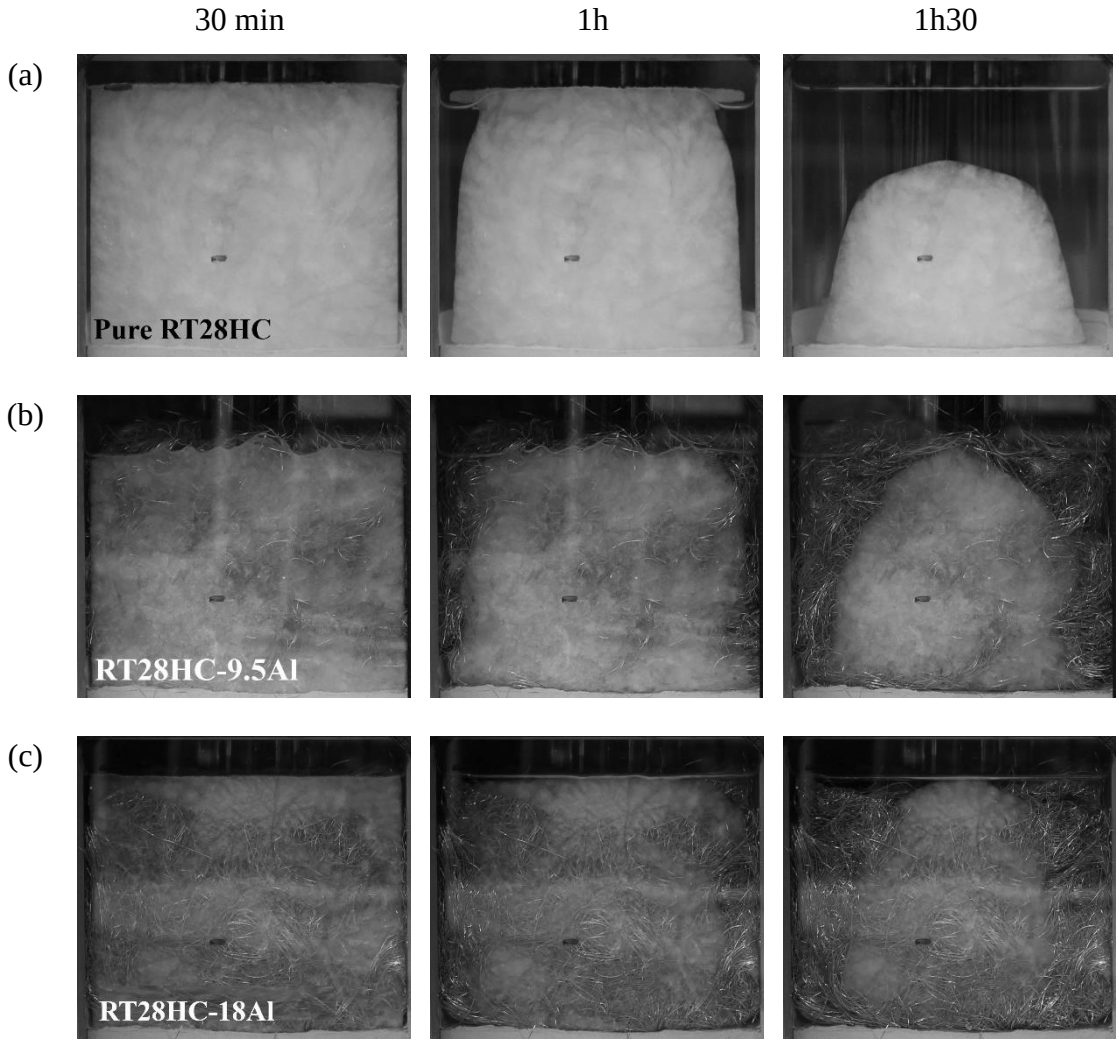

Figure 6: Evolution of the melting of (a) pure RT28HC (b) RT28HC-9.5Al (c) RT28HC-18Al at 0.15A. Solid RT28HC is opaque white and becomes transparent in liquid phase.

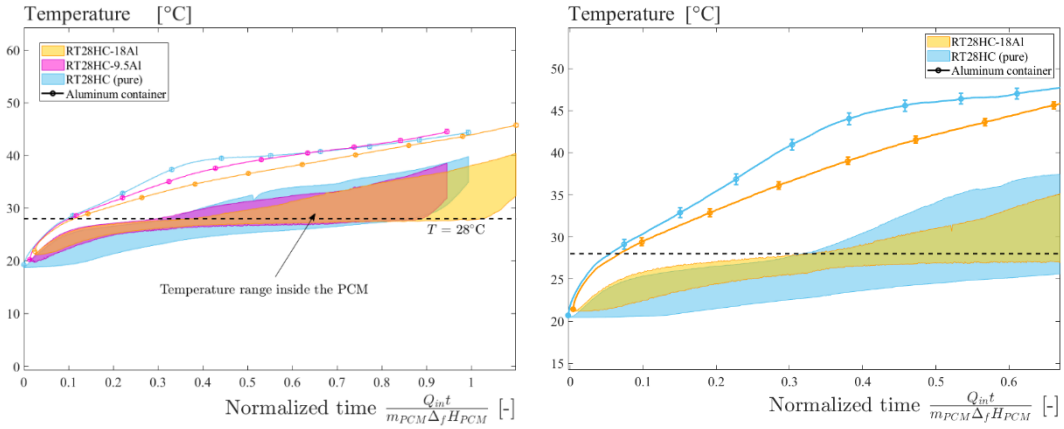

Figure 7: Temperature evolution during melting experiment for the different hybridized PCM compositions (left: applied current 0.15A – right: applied current 0.25A). The lines are mean values of the temperature measurements on the aluminum container, the solid shape corresponds to the range of the temperatures measured inside the PCM. The boundaries correspond to the innermost and outermost thermocouples.

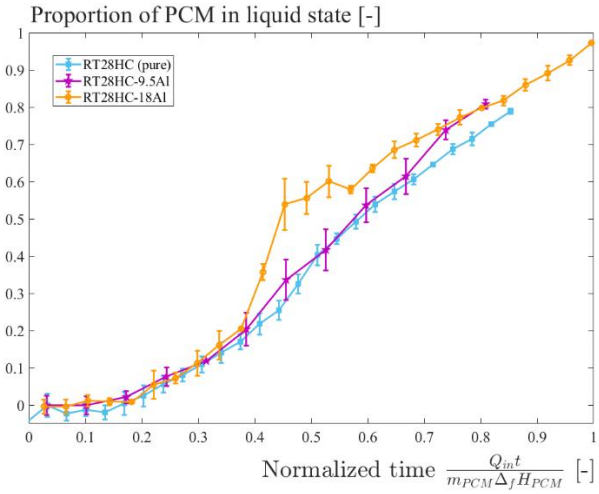

Figure 8: Evolution of the quantity of PCM in liquid state for experiments at 0.15A. The mass in solid state has been determined from contour measurements on the pictures considering axial symmetry around the vertical axis and the experimentally measured solid state density.

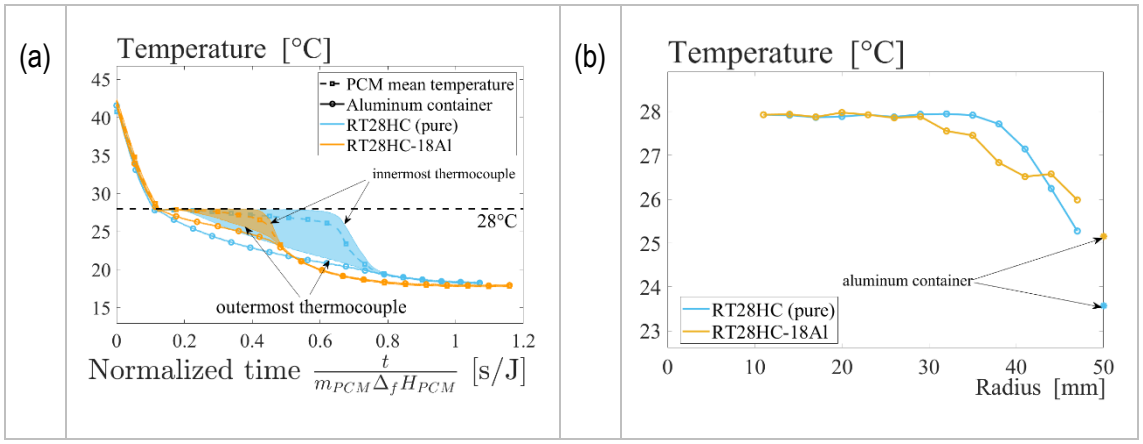

Figure 9: (a) Temperature evolution during solidification experiment by free cooling for the different hybridized PCM compositions. (b) Radial temperature profile inside the sample at $t/m_{PCM}\Delta_f H_{PCM}$ *= 0.35 s/J.*

4. Discussion

4.1. Thermal conductivities of the hybridized PCM

a. In solid phase

In solid phase the apparent thermal conductivity can be considered as equal or very close to the actual thermal conductivity of the composite because there are no convection effects.

The thermal conductivity of pure solid RT28HC equal to 0.5 ± 0.1 W/(m·K) is higher than expected from the datasheet (0.2 W/m·K). The duration of the transient regime is approximatively equal to 5 $R^2/(D\ \lambda_1^2)$. This corresponds to nearly 30 min. Therefore, the current has been decreased in some experiments involving a low thermal diffusivity in order to keep the outermost temperature below phase change during a sufficiently long time period, especially in the case RT28HC. However, the duration of the stationary regime is still too short to deliver accurate values of the thermal conductivity in the latter case. Moreover, since the solidification is associated with a

volume change and begins from the sides, there are some voids left in the center, as it is confirmed by the actual density which is a little lower than the datasheet value. The c_p value used for calculations is hence overestimated since it does not consider the presence of air, and this explains that k is overestimated as well.

Several homogenization models exist for evaluating the thermal conductivity of the hybrid, bound by the in-series and in parallel model. Most of them are based on a 3D regular cell model. A list of such models is given in [32]. Several among these models are based on cell geometry parameters and hence cannot be applied on the wool-PCM composite. However, some models depend on porosity only such as the Maxwell-Euken model [32] or the ones of Singh et al. [33], Boomsma et al. [32] or Mesalhy et al. [34]. The predictions obtained with these models are represented in Figure 10 along with experimental data out of the literature for aluminum foams infiltrated with paraffin PCM [17,35]. The values for steel wool infiltrated with epoxy resin provided in [26] have been added for comparison, too. As for aluminum foam hybrided PCM, the thermal conductivity of wool-hybrided PCM is enhanced by one order of magnitude with respect to pure PCM. However, the increase of the thermal conductivity is more important in the case of foams compared to wool. Contrary to a foam, a wool is not a totally percolating medium and thermal resistances arise at the contact points, which explains the lower thermal conductivity. The presence of air inside the RT28HC-18Al sample also decreases the resultant thermal conductivity. The results of the present study are in line with the results of Prieto and al. measured on a steel wool-epoxy compound [26]. Stainless steel has a 10 times lower thermal conductivity than aluminum and hence a smaller improvement of the overall thermal conductivity was expected. However, in their study, the fibers were oriented in the heat flow direction whereas in our case the fibers were

randomly distributed. Khliyeva et al. [36] measured the thermal conductivity of aluminum wool – paraffin composites and obtained a lower thermal conductivity as in the present study for equivalent aluminum wool content. However, their samples were 100 times smaller and metal mass ratio was also much smaller, such that homogeneity of the fiber distribution and orientation might have been different compared to ours. The fiber diameter was equal to 30 µm compared to 100 µm here, which could also explain the differences.

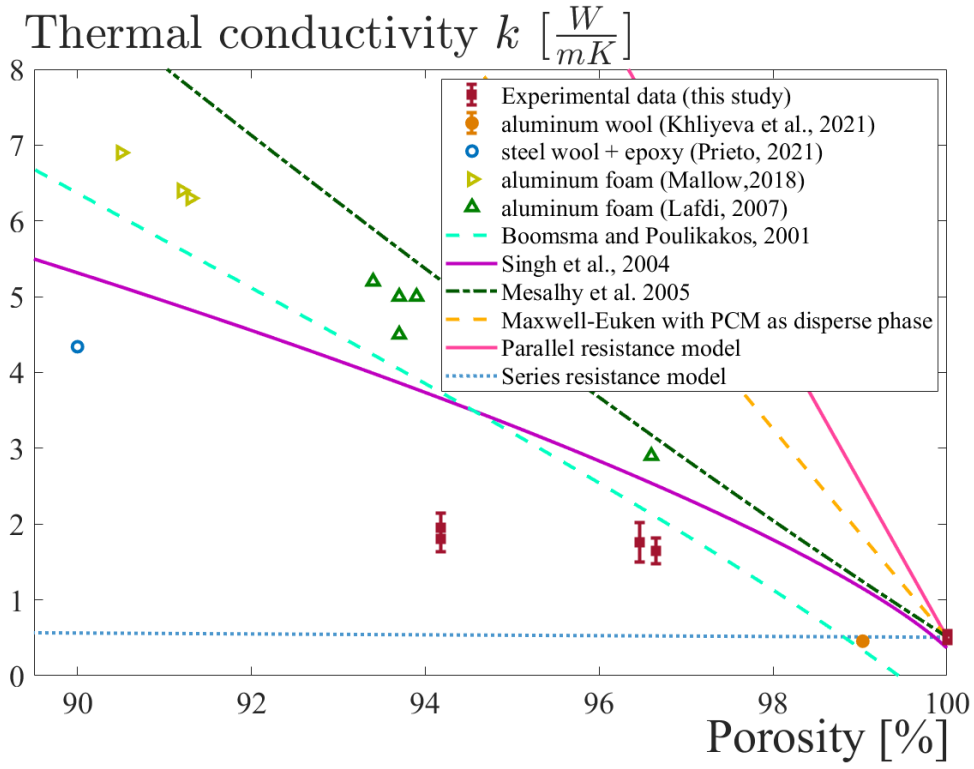

Figure 10: Experimental values of the thermal conductivity of the wool-PCM composite in solid phase compared to predictions of analytical homogenization models, combined with experimental data for paraffin-aluminum foam composites.

b. In liquid phase

For pure RT28HC, the apparent thermal conductivity in liquid phase is 20 times larger than in solid phase. Contrary to the solid phase, the conductivity measured in the liquid phase is an apparent conductivity due to the presence of convection phenomena. Temperature homogenization effects and enhanced heat transfer due to natural convection have already been found in similar experiments or simulations with PCM in [14,15,24]. Evidence of the presence of natural convection can also be found in Figure 6 in which the dome-shaped fusion front shows that the temperature is larger in the top region compared to the bottom region. The fusion front is more vertical in the presence of wool, due to prevention of the convection movements.

Natural convection phenomena do not occur in solid phase, while in the liquid phase they are dependent on the enclosure design. However, the enclosure design is the same for all specimens. Therefore, the ratio k_{liq}/k_{sol} displayed in Figure 11 reflects the effect of the addition of wool on the intensity of the heat transfer due to convection phenomena. Nevertheless, the absolute quantitative value is valid for our set-up only.

The high uncertainty on the value for pure RT28HC in liquid phase is due to the fact that the temperature differences between the different radii are in the order of magnitude of the thermal noise, leading to a large uncertainty on the slope when performing the linear interpolation. However, the present study is mainly focused on the differences between specimens rather than on the absolute values. Note that the set-up has not been designed to measure the thermal conductivity, and this explains the uncertainties. The variations are much larger than the uncertainties.

The apparent thermal conductivity increases with the addition of the metallic wool in solid phase, but decreases in liquid phase, which leads to a decreasing k_{liq}/k_{sol} ratio with

increasing wool content. For the highest Al wool content, there is no statistically significant difference between the liquid and the solid phase, which indicates that fluid movements are totally prevented. The logarithmic scale in Figure 11 indicates that a significant loss of apparent conductivity takes place already for small Al wool contents. Prieto et al. [24] estimated roughly the improvement of heat transfer by a factor 10 owing to natural convection for a porosity of 98.5% (corresponding here to 4.8% aluminum mass content), which is in line with our results.

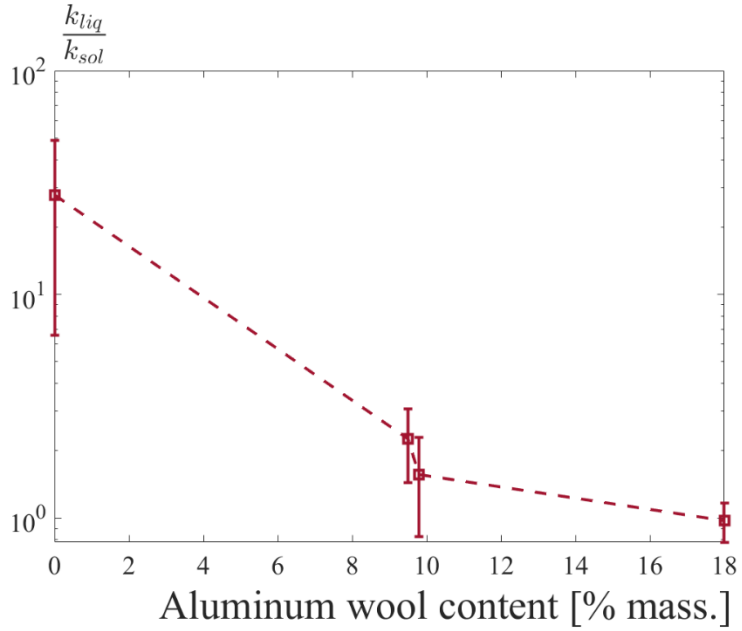

Figure 11: Ratio of the apparent thermal conductivities measured in liquid and in solid phase.

4.2. Effect of the metallic wool on phase change

First, the melting process is addressed. The value for Q^{in} determined by equation (4) is equal to 7.6 ± 1.0 W and 14.0 ± 2.5 W (see Figure 3), respectively, for applied current equal to 0.15A and 0.25A. An approximative 10% variation is observed in the value of Q^{in} in the middle of the experiment duration, although the current going through the

Peltier elements is constant. Indeed, during phase change, the temperature of the container stays almost constant and hence does not consume power in order to heat up, contrary to the beginning and the end of the experiment, where the temperature of the container rises. However, this occurs at the same time for all specimens, hence, the comparison remains valid. The shape of the fusion front has already been discussed in the previous section. The comparison of the position of the fusion front with the measured temperatures shows that the fusion front follows the 28-29°C isotherms. When adding the Al wool, the solid phase becomes greyish and distinguishing between the liquid and solid phase gets much more difficult, especially for the RT28HC-18Al. Indeed, the radial temperature gradient is small in solid phase due to the better conductivity of the solid. Due to the increased thermal conductivity in the hybridized PCM, the solid phase melts much more homogeneously and therefore the solid block is actually a mixture of solid and liquid, which explains why the fusion front is not so well defined.

Figure 7 shows the temperature evolution for the different PCM compositions. The time has been normalized by the time necessary to melt the entire sample in homogeneous conditions. Note that the thermocouples are located at half height of the sample, and hence they capture the behavior at that specific position, which differs from the one at other heights in the presence of convection effects.

At first sight, it could have been be expected that the enhanced thermal conductivity of the composite would lead to a lower aluminum container temperature in the wool-added systems compared to pure PCM. This is indeed what was found in [16] in the case of a foam-added material. However, Figure 7 shows that the temperature of the container rises first faster without the wool, but after some time the container temperature reaches a plateau. On the other hand, the case without wool the temperature continuously rises.

At the end of the melting process, there is no significant difference between the systems with and without wool. This is true for the two tested heat flows. This is due to the competing effect between thermal conductivity enhancement by the wool in solid phase and the loss of natural convection in the liquid phase. Khliyeva et al. [36] proposed a similar explanation for metallic wool-paraffin composites based on the temperature curves but without visual confirmation. Figure 8 shows the amount of PCM which has molten as determined from the pictures. Note that the amount of liquid in the hybrided cases is underestimated since only transparent areas are considered as molten. In the cases with wool, the PCM is greyish which indicates that it is partially molten. The gain in melting times when adding wool remains limited, again due to the loss of natural convection in the liquid phase.

Although in the melting configuration, the addition of wool does not bring important improvement on the limitation of the container temperature or in the amount of stored energy, in the solidification configuration, the addition of wool reduces the solidification time by a factor of 2, as it is exhibited in Figure 9(a).

The reason for this asymmetric behavior is related to the direction of the heat flow with respect to the position of liquid and solid phases. In the melting configuration, heat must first go through the liquid phase before reaching the fusion front, then it must penetrate the solid. Without wool, the rate-limiting step is the heat conduction inside the solid, hence the heat reaches quite easily the fusion front. At the beginning, when there is less liquid phase, the lower conduction in the pure PCM generates a temperature rise at the larger radii and in the container, but this effect is limited when further liquid phase forms. Hence, the difference between the maximum and minimum temperature remains almost constant and the container temperature reaches a plateau, as observed in Figure 7.

In the RT28HC-18Al sample, there is no real rate-limiting step, since conduction in liquid and in solid is identical. This explains that the temperature homogeneously rises until about a half of the PCM is melted (characteristic time around 0.4). However, once a significant amount of liquid phase is present, the hybrided PCM sample becomes less efficient compared to the sample without wool because of the improved heat transfer by convection in the latter case. The container temperature keeps rising and finally reaches the one of the sample without wool. In the solidification configuration, the situation is inverted: heat is withdrawn from the periphery of the sample and the outer part of the sample solidifies first. In the case of the pure PCM sample, this solid ring constitutes an obstacle for the heat contained in the center to flow out, which can be related to the sharp temperature gradient in Figure 9(b). As a consequence, the container temperature goes down faster than in the case with wool (see Figure 9(a)). Since the outgoing heat flow is proportional to the difference between the container temperature and the room temperature, it is smaller in the absence of wool, leading to increased time for complete solidification. Indeed, Figure 9(a) shows that the solidification process takes about 0.33 s/J for the hybridized PCM, whereas it takes about 0.55 s/J for the pure PCM. Solidification experiments using the Peltier elements for withdrawing the heat have been performed as well. The conclusions are the same, except that in this case the heat flow is fixed and it is the container temperature which sharply decreases down in the absence of wool. Yang et al. [21] showed that there is a contribution of natural convection also in solidification experiments. Nevertheless, in our experiments, this contribution in the melting configuration is too small to counterbalance the benefit of the wool enhanced heat conduction in the solid phase.

Other mechanisms could also lead to an asymmetric behavior between solidification and melting, such as for instance an influence of the thermal history, a rate dependent crystallization, an enhanced germination in the presence of wool. Hence, in order to prove that the experimentally observed asymmetric behavior is indeed mainly related to the natural convection, FE simulations of melting and solidification have been performed with a symmetric enthalpy curve centered on the fusion temperature. Heat transfer by convection in the liquid phase has been taken into account artificially by using a higher thermal conductivity in the liquid phase, as it has already be proposed in the study of Prieto et al. [24]. The thermal conductivity has been set as temperature dependent related linearly to the mass fraction of melted PCM $x_{liq}(T)$:

$$k(T) = \begin{cases} k_{sol} \text{ for } x_{liq}(T) < x_{thres} \\ k_{sol} + \dfrac{k_{liq} - k_{sol}}{1 - x_{thres}} \left(x_{liq}(T) - x_{thres}\right) \text{ for } x_{liq}(T) < x_{thres} \end{cases}, \quad (5)$$

where k_{sol} and k_{liq} are respectively the thermal conductivity of the solid and liquid phases. The threshold value x_{thres} = 50% has been selected in order to reproduce the plateau behavior observed previously and expresses that a minimum quantity of liquid is necessary for the natural convection to take place.

A homogeneous initial temperature is set 10°C below and above fusion temperature in melting and solidification configurations, respectively. Figure 12 represents the difference between the temperature at the external periphery of the PCM with respect to the mean temperature in the PCM. Values of the thermal conductivities mimic the values found for the different test configurations. The mean temperature evolution depends only on the ingoing/outgoing heat flow and the enthalpy curve and is hence independent of the values of the thermal conductivity and on the heat flow direction. PCM with infinite heat conduction corresponds to T_{ext}-T_{mean} =0°C. As is it can be seen in Figure 12 where the

curves are perfectly superposed, when $k_{liq}=k_{sol}$ due to the symmetry of the enthalpy curve and the initial temperature: $(T_{ext} - T_{mean})_{solidification} = -(T_{ext} - T_{mean})_{melting}$. When the ratio k_{liq}/k_{sol} increases, the asymmetry between solidification and melting configuration becomes more important. The behavior of the RT28HC-9.5Al (Q^{in}/k_{sol} = 4.6 K·m, k_{liq}/k_{sol} = 2.5) and RT28HC-18Al (Q^{in}/k_{sol} = 4.3 K·m, k_{liq}/k_{sol} = 1) configurations are very close, despite nearly two times more wool volume fraction: the loss of performance of the RT28HC-9.5A at the end of solidification and at the beginning of melting is negligible.

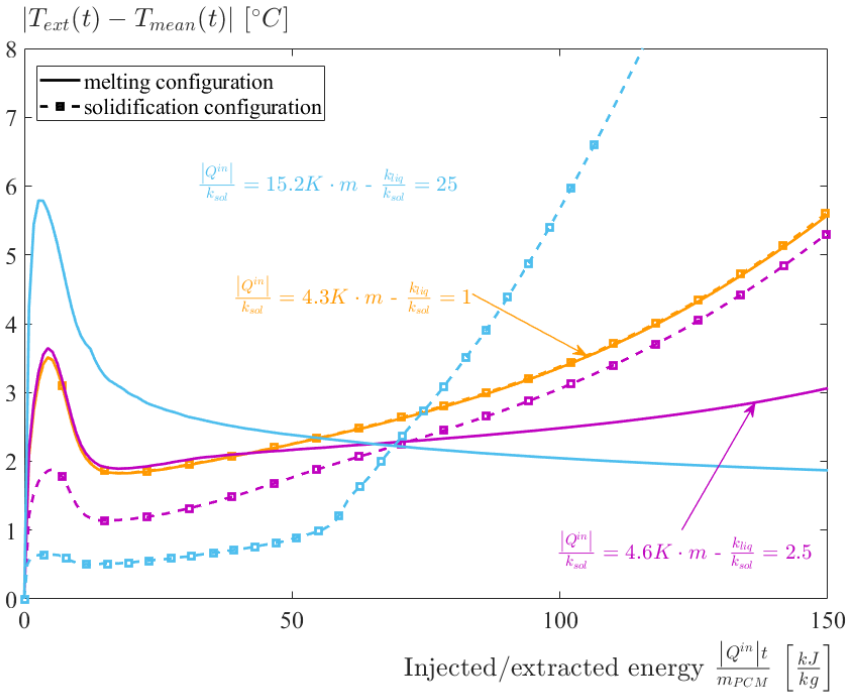

Figure 12: Difference between the temperature at the external boundary of the PCM and the mean temperature of the PCM for different combinations of liquid and solid thermal conductivities. Data is represented in melting (continuous line) and solidification (dashed line with marker) configuration. As a guide for the eye, the values of the meting configuration have been mirrored with respect to the x-axis.

Both charge (melting) and discharge (solidification) behaviors are important to consider when designing a heat storage system. For instance, in temperature control systems in buildings, PCMs are used to partly or entirely avoid climatization. In a charging configuration, a fixed heat flow enters the room and the room temperature has to be kept low. Comparatively, this corresponds in our experimental set-up to the melting configuration and the container temperature reflects the behavior of the temperature inside the building. In discharging configuration, PCM solidifies overnight by natural convection, and has to be solid at the end of the night. With regard to this specific application, addition of wool has a slightly positive effect on the charging configuration, but greatly enhances the discharging times.

A building wall of thickness w containing a material able to melt may store a quantity $w\rho\Delta_f H$ of energy per unit area. At fixed melting, inner and outer temperatures, charging and discharging times is mainly proportional to $w^2\rho\Delta_f H/k$. Following the rationale material selection approach, maximization of the stored energy while keeping charging and discharging times below a fixed duration imposes to maximize $\sqrt{k\rho\Delta_f H}$. The apparent thermal conductivity to be used is the worst one, hence during solidification where heat transfer is not potentially enhanced by natural convection. With regard to this case, wool hybrided PCMs are better than pure PCMs despite the prevention of the natural convection effects. Nevertheless, this analysis does not take cost into account. The evolution of the performance is not linear with the proportion of wool, and there is an optimum to be found with respect to the performance of the compound and the additional cost. Also, from the conductivity values shown in Figure 10, foam hybrided PCMs show a little better performance at equal metal content compared to wool, however price difference between wools and foams and ease of process of wools compensate this.

5. Conclusion

The effect of adding metallic wool as a cheap and easy to process heat transfer enhancement principle of PCMs has been investigated. Using a single home-made set-up at fixed heat flows, the thermal conductivity of organic PCM hybridized with aluminum wool has been measured and the phase change behavior has been studied in both melting and solidification configurations.

The addition of small quantities of aluminum wool (less than 20% mass) enhances the thermal conductivity by a factor 20 with respect to the pure PCM. The contact thermal resistance between the fibers limit the conductivity gains compared to percolating matrices such as foams.

The addition of wool does not have an important effect on the outer temperature in the melting configuration because the gain in thermal conductivity in solid phase is countered by the loss of thermal convection in the liquid phase. The experiments have highlighted an asymmetric behavior between melting and solidification in pure PCM because convection does not allow a better heat transfer in the solidification configuration. There is a critical amount of wool content where thermal conductivity in solid phase is improved and liquid and solid phase show similar apparent heat conductivities, which will lead to a more symmetric behavior between charging and discharging cycles. As a consequence, an optimum between asymmetry of the behavior and amount of wool has to be determined as a function, in particular, of the needed performances, the price of the wool and the available volume.

This study confirms that the heat transfer enhancement offered by the addition of metallic wool in PCM is similar to the addition of a metallic foam, however metallic wools are cheaper and easier to process than foams. Heat transfer behaves in a similar

way, and therefore previous studies on PCM-foam composites can easily be applied to PCM-wool composites in order to design efficient heat storage. Further studies should focus on the optimization of the wool parameters such as the fiber diameter or section shape so as to reduce the contact resistances and to keep the advantages of natural convection in liquid phase.

The first order rationale material selection approach applied to a building wall performed in this study shows the added value of hybriding PCMs with wool for heat storage applications. Nonetheless, a more systematic material selection approach should be applied with respect to selected applications in order to select the best PCM hybriding method considering also the ease and cost of process and the desired characteristic times at melting and solidification.

6. Acknowledgements

The authors acknowledge the financial support of the European Fund for Regional Development and the Walloon Region through the FEDER-STOCC project.

7. References

[1] Y. Lin, Y. Jia, G. Alva, G. Fang, Review on thermal conductivity enhancement, thermal properties and applications of phase change materials in thermal energy storage, Renew. Sustain. Energy Rev. 82 (2018) 2730–2742. https://doi.org/10.1016/j.rser.2017.10.002.

[2] N.I. Ibrahim, F.A. Al-sulaiman, S. Rahman, B.S. Yilbas, Z. Sahin, Heat transfer enhancement of phase change materials for thermal energy storage applications : A critical review, Renew. Sustain. Energy Rev. 74 (2017) 26–50. https://doi.org/10.1016/j.rser.2017.01.169.

[3] C.Y. Zhao, W. Lu, Y. Tian, Heat transfer enhancement for thermal energy storage using metal foams embedded within phase change materials (PCMs), Sol. Energy. 84 (2010) 1402–1412. https://doi.org/10.1016/j.solener.2010.04.022.

[4] T. Oya, T. Nomura, N. Okinaka, T. Akiyama, Phase change composite based on porous nickel and erythritol, Appl. Therm. Eng. 40 (2012) 373–377. https://doi.org/10.1016/j.applthermaleng.2012.02.033.

[5] M. Karthik, A. Faik, B.D. Aguanno, Solar Energy Materials and Solar Cells Graphite foam as interpenetrating matrices for phase change para ffi n wax : A candidate composite for low temperature thermal energy storage, Sol. Energy Mater. Sol. Cells. 172 (2017) 324–334. https://doi.org/10.1016/j.solmat.2017.08.004.

[6] Z. Song, Y. Deng, J. Li, H. Nian, Expanded graphite for thermal conductivity and reliability enhancement and supercooling decrease of MgCl2·6H2O phase change material, Mater. Res. Bull. (2018). https://doi.org/10.1016/j.materresbull.2018.02.024.

[7] V. Kumaresan, R. Velraj, S.K. Das, The effect of carbon nanotubes in enhancing the thermal transport properties of PCM during solidification, Heat Mass Transf. Und Stoffuebertragung. 48 (2012) 1345–1355. https://doi.org/10.1007/s00231-012-0980-3.

[8] C.J. Ho, J.Y. Gao, An experimental study on melting heat transfer of paraffin dispersed with Al2O3 nanoparticles in a vertical enclosure, Int. J. Heat Mass Transf. 62 (2013) 2–8. https://doi.org/10.1016/j.ijheatmasstransfer.2013.02.065.

[9] S. Motahar, A.A. Alemrajabi, R. Khodabandeh, Experimental study on solidification process of a phase change material containing TiO 2 nanoparticles

for thermal energy storage, Energy Convers. Manag. 138 (2017) 162–170. https://doi.org/10.1016/j.enconman.2017.01.051.

[10] Q. Ren, F. Meng, P. Guo, A comparative study of PCM melting process in a heat pipe-assisted LHTES unit enhanced with nanoparticles and metal foams by immersed boundary-lattice Boltzmann method at pore-scale, Int. J. Heat Mass Transf. 121 (2018) 1214–1228. https://doi.org/10.1016/j.ijheatmasstransfer.2018.01.046.

[11] H. Badenhorst, A review of the application of carbon materials in solar thermal energy storage, Sol. Energy. 192 (2019) 35–68. https://doi.org/10.1016/j.solener.2018.01.062.

[12] X. Xiao, P. Zhang, M. Li, Effective thermal conductivity of open-cell metal foams impregnated with pure paraffin for latent heat storage, Int. J. Therm. Sci. 81 (2014) 94–105. https://doi.org/10.1016/j.ijthermalsci.2014.03.006.

[13] J. Baumeister, J. Weise, S. Myslicki, E. Kieseritzky, G. Lindenberg, Pcm-based energy storage system with high power output using open porous aluminum foams, Energies. 13 (2020) 1–17. https://doi.org/10.3390/en13236198.

[14] R.E. Murray, D. Groulx, Experimental study of the phase change and energy characteristics inside a cylindrical latent heat energy storage system: Part 1 consecutive charging and discharging, Renew. Energy. 62 (2014) 571–581. https://doi.org/10.1016/j.renene.2013.08.007.

[15] J.M. Mahdi, E.C. Nsofor, Multiple-segment metal foam application in the shell-and-tube PCM thermal energy storage system, J. Energy Storage. 20 (2018) 529–541. https://doi.org/10.1016/j.est.2018.09.021.

[16] A. Diani, M. Campanale, Transient melting of paraffin waxes embedded in

aluminum foams: Experimental results and modeling, Int. J. Therm. Sci. 144 (2019) 119–128. https://doi.org/10.1016/j.ijthermalsci.2019.06.004.

[17] K. Lafdi, O. Mesalhy, S. Shaikh, Experimental study on the influence of foam porosity and pore size on the melting of phase change materials, J. Appl. Phys. 102 (2007). https://doi.org/10.1063/1.2802183.

[18] Y. Yao, H. Wu, Thermal transport process of metal foam/paraffin composite (MFPC) with solid-liquid phase change: An experimental study, Appl. Therm. Eng. 179 (2020) 115668. https://doi.org/10.1016/j.applthermaleng.2020.115668.

[19] M. Martinelli, F. Bentivoglio, A. Caron-soupart, Experimental study of a phase change thermal energy storage with copper foam, Appl. Therm. Eng. 101 (2016) 247–261. https://doi.org/10.1016/j.applthermaleng.2016.02.095.

[20] Y.B. Tao, Y. You, Y.L. He, Lattice Boltzmann simulation on phase change heat transfer in metal foams/paraffin composite phase change material, Appl. Therm. Eng. 93 (2016) 476–485. https://doi.org/10.1016/j.applthermaleng.2015.10.016.

[21] X. Yang, Q. Bai, Q. Zhang, W. Hu, L. Jin, J. Yan, Thermal and economic analysis of charging and discharging characteristics of composite phase change materials for cold storage, Appl. Energy. 225 (2018) 585–599. https://doi.org/10.1016/j.apenergy.2018.05.063.

[22] S. Venettacci, R. Cozzolino, G.S. Ponticelli, S. Guarino, Environmental and economic life cycle assessment of thermal energy storage based on organic phase change material embedded in open-cell copper foams, Sustain. Prod. Consum. 29 (2022) 387–405. https://doi.org/10.1016/j.spc.2021.10.026.

[23] Ekksol, Production steel wool, (n.d.). https://ekksol.com/production-steel-wool.

[24] C. Prieto, C. Rubio, L.F. Cabeza, New phase change material storage concept

1 including metal wool as heat transfer enhancement method for solar heat use in
2 industry, J. Energy Storage. 33 (2021) 101926.
3 https://doi.org/10.1016/j.est.2020.101926.
4 [25] H. Wang, F. Wang, Z. Li, Y. Tang, B. Yu, W. Yuan, Experimental investigation
5 on the thermal performance of a heat sink filled with porous metal fiber sintered
6 felt/paraffin composite phase change material, Appl. Energy. 176 (2016) 221–232.
7 https://doi.org/10.1016/j.apenergy.2016.05.050.
8 [26] C. Prieto, A. Lopez-Roman, N. Martínez, J.M. Morera, L.F. Cabeza, Improvement
9 of phase change materials (PCM) used for solar process heat applications,
10 Molecules. 26 (2021). https://doi.org/10.3390/molecules26051260.
11 [27] J. Gasia, J.M. Maldonado, F. Galati, M. De Simone, L.F. Cabeza, Experimental
12 evaluation of the use of fins and metal wool as heat transfer enhancement
13 techniques in a latent heat thermal energy storage system, Energy Convers. Manag.
14 184 (2019) 530–538. https://doi.org/10.1016/j.enconman.2019.01.085.
15 [28] M. Velasco-Carrasco, Z. Chen, J.L. Aguilar-Santana, S. Riffat, Experimental
16 evaluation of phase change material blister panels for building application, Futur.
17 Cities Environ. 6 (2020) 1–7. https://doi.org/10.5334/fce.84.
18 [29] M.S. Yousef, H. Hassan, Energetic and exergetic performance assessment of the
19 inclusion of phase change materials (PCM) in a solar distillation system, Energy
20 Convers. Manag. 179 (2019) 349–361.
21 https://doi.org/10.1016/j.enconman.2018.10.078.
22 [30] M.F. Ashby, Materials Selection in Mechanical Design, 5th ed., Pergamon Press,
23 2016.
24 [31] W.Q. Li, Z.G. Qu, B.L. Zhang, K. Zhao, W.Q. Tao, Thermal behavior of porous

stainless-steel fiber felt saturated with phase change material, Energy. 55 (2013) 846–852. https://doi.org/10.1016/j.energy.2013.02.064.

[32] P. Zhang, X. Xiao, Z.W. Ma, A review of the composite phase change materials : Fabrication, characterization, mathematical modeling and application to performance enhancement, Appl. Energy. 165 (2016) 472–510. https://doi.org/10.1016/j.apenergy.2015.12.043.

[33] R. Singh, H.S. Kasana, Computational aspects of effective thermal conductivity of highly porous metal foams, Appl. Therm. Eng. 24 (2004) 1841–1849. https://doi.org/10.1016/j.applthermaleng.2003.12.011.

[34] O. Mesalhy, K. Lafdi, A. Elgafy, K. Bowman, Numerical study for enhancing the thermal conductivity of phase change material (PCM) storage using high thermal conductivity porous matrix, Energy Convers. Manag. 46 (2005) 847–867. https://doi.org/10.1016/j.enconman.2004.06.010.

[35] A. Mallow, O. Abdelaziz, S. Graham, Thermal charging performance of enhanced phase change material composites for thermal battery design, Int. J. Therm. Sci. 127 (2018) 19–28. https://doi.org/10.1016/j.ijthermalsci.2017.12.027.

[36] O. Khliyeva, V. Zhelezny, A. Paskal, Y. Hlek, D. Ivchenko, The effect of metal wool on the charging and discharging rate of the phase transition thermal storage material, Eastern-European J. Enterp. Technol. 4 (2021) 12–20. https://doi.org/10.15587/1729-4061.2021.239065.